ACS APPLIED MATERIALS & INTERFACES

www.acsami.org

Research Article

Nanoscale Nickel-Based Thin Films as Highly Conductive Electrodes for Dielectric Elastomer Applications with Extremely High Stretchability up to 200%

Jonas Hubertus,* Julian Neu, Sipontina Croce, Gianluca Rizzello, Stefan Seelecke, and Günter Schultes

Cite This: *ACS Appl. Mater. Interfaces* 2021, 13, 39894−39904

Read Online

ACCESS | Metrics & More | Article Recommendations | Supporting Information

ABSTRACT: This paper presents on electromechanical characterization of thin film nickel-based wrinkled electrodes for dielectric elastomer (DE) applications. The investigation of a sandwich composed of a very soft and flexible elastomer carrying an ultrathin metallic electrode, together with its prestretch-dependent wrinkled structure of the electrode, facilitates the understanding of some of its interesting properties. Compared to conventional screen-printed carbon black electrodes, nickel-based thin film electrodes offer an ohmic resistance that is about 2 orders of magnitude lower. This remarkable feature makes it an advantageous electrode material alternative for the development of energy-efficient and high-frequency DE applications. Ultrathin (10−20 nm) layers are sputter deposited as electrodes onto either biaxially or, under pure-shear conditions, uniaxially prestretched silicone membranes. After the sputtering process, the membranes are allowed to relax whereby wrinkled out-of-plane buckled surfaces are obtained. With an initial resistance smaller than 400 Ω/square and a strong adhesion to the silicone, some electrode configurations are able to withstand strains up to 200% while remaining electrically conductive. A linear dependence of the capacitance on strain is revealed, as well as a long-term stability over 10 million cycles of mechanical stretching. All investigated thin film configurations of nickel and nickel−carbon films are suitable as compliant electrodes for DE actuators, as demonstrated by measuring the force characteristics with and without a high voltage. An increased level of prestretch shifts the resistance threshold of the electrode layers to even higher strain levels. In general, the best performance is achieved with pure metallic electrodes deposited on biaxially prestretched silicone membranes.

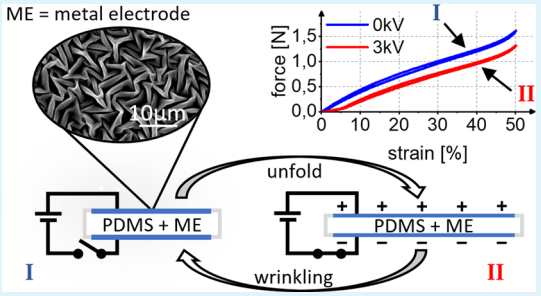

KEYWORDS: *compliant electrode, sputtered thin film, wrinkles, dielectric elastomer, metallic electrode, electromechanical characterization*

INTRODUCTION

A dielectric elastomer (DE) is a thin elastomeric membrane, often made of transparent and soft silicone polymers, sandwiched between two compliant electrodes. In this way, an electroactive system emerges that resembles a flexible parallel plate capacitor. Such a kind of DE represents a relatively new type of electromechanical transducers.[1] By applying a high voltage between the electrodes, electrical energy can be converted into mechanical work for actuation purposes. This phenomenon occurs due to the fact that the electric field causes an attraction between the electrodes, which, in turn, squeezes the membrane in between and makes it elongate in-plane.[2] Several DE actuator concepts such as loudspeakers,[3,4] optical lenses,[5,6] artificial muscles,[7,8] smart skins,[9] and others can be found in the literature. Other than actuators, energy-harvesting systems can also be realized with DEs, thus allowing to convert mechanical energy into electrical one.[10−12] Furthermore, during the deformation of the DE, the resistance and the capacitance change accordingly, and hence a DE can be used as a sensor as well.[13−16] DE applications combine extraordinary properties such as large deformations, lightweight, silent operation, scalability, energy efficiency, and self-sensing capabilities.[17−19]

High-performance DE systems require highly compliant and low-resistance electrodes with a negligible mechanical influence on the soft elastomer. Properties such as an extraordinary fatigue behavior, high flexibility and stretchability, and ability to remain conductive while being deformed are also needed.[17] Today, carbon-black (CB) material is often used for designing compliant electrodes of DEs. Despite the relatively high electrical resistance (50 kΩ/square) of typically used CB electrodes, these are still highly attractive for a number of practical reasons. For instance, screen printing represents a well-established and easily controlled method to manufacture CB electrodes, which facilitates the mass

Received: June 8, 2021
Accepted: July 15, 2021
Published: August 10, 2021

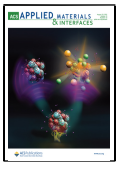

production of rather macroscopic DE.[2,17,20−24] Metal electrodes can be seen as a complementary alternative for future miniaturized DE applications. Furthermore, the low resistance of such electrodes in combination with a low RC-constant is advantageous regarding high-frequency actuation, sensing, and self-sensing.[25] Also, the efficiency of energy harvesters can be improved.[26] Unfortunately, the stretchability of metal electrodes is limited because the low elasticity of metals, combined with a high Young's modulus, stiffen the overall system. Different ideas were realized to overcome these drawbacks. As relevant examples, thin film-coated corrugated surfaces[27] or wrinkled electrodes[28−30] were developed to achieve electrodes with a stretchability of 80% linear strain and 120% of radial strain, respectively. Other publications report about meander structures,[31−33] zig-zag patterns,[2] kirigami techniques,[34] and metal nanowire-based electrodes.[35,36]

Wrinkles, understood as out-of-plane buckled surfaces, are well known to provide flexibility and stretchability. Their effects have been studied in the DE field,[37,38] as well as in the area of stretchable and flexible electronics.[39,40] In our work, the systematic creation of wrinkles, obtained by coating an either biaxially or under pure shear condition (PSC) uniaxially prestretched silicone membranes, is used to achieve a compliant electrode for electroactive polymer applications. After performing the sputter deposition of the electrode onto the prestretched membrane, the silicone is allowed to relax and wrinkles are formed. When such a wrinkled electrode is stretched, the wavy surface is first flattened before a larger deformation beyond the prestretch level starts to stress the metal electrode itself. The stretchable wrinkle structure acts as a mechanical buffer. Therefore, we try to combine this kind of geometrical buffer with new—thin film-based—low-resistive electrode materials in order to enlarge the application range and, at the same time, to enable the miniaturization of DE systems. New electrode materials are explored in this study. Thin film nickel, nickel−carbon, and carbon−nickel sandwich electrodes are investigated for this purpose. The unusual material selection for flexible electrodes is inspired by our own previous work on compliant NiCr−carbon electrodes[41] and strain sensors of metal−carbon layers.[42,43] Carbon sometimes offers unexpected and unique material properties as it can be seen in our previous work. Based on this, we assume that different electrode configurations should reveal different electromechanical properties for the nickel-based electrodes as well. As an important step, new results of the electromechanical performance of nickel-based electrodes are presented in this paper.

MATERIALS AND METHODS

Materials and Preparation. All experiments are carried out with electrodes deposited onto Wacker Elastosil 2030 250/50 silicone films. The thickness of these elastomeric membranes was measured, resulting into a value of 47.5 μm ± 5%. The membrane exhibits a dielectric strength of 80−100 V/μm, an elongation at break of 450%, and a dielectric constant of 2.8.[44]

At the beginning of the process, the membrane is removed from the carrier film, then prestretched to a certain degree, and fixed on a metal rack in the prestretched state. Either an 8 × 8 cm^2 marked square is elongated to an 11 × 11 cm^2 square, or a 7 × 7 cm^2 square is lengthened to an 11 × 7 cm^2 rectangle. The preload ratios correspond to a 37.5% equibiaxial prestretch, or to a 57.5% uniaxial prestretch applied under PSCs, respectively. These discrete levels of prestretch (LoP) are chosen for practical reasons, and originate from the dimensions of the metal rack. In this study, almost all deposition processes are carried out on membranes prestretched with these two LoPs. In addition, one set of experiments is conducted with specimens of increased LoP. In this case, a 7 × 7 cm^2 square is stretched to 11 × 11 cm^2, hence, 57.5% equibiaxial, or a 6 × 7 cm^2 rectangle is lengthened to an 11 × 7 cm^2 rectangle, resulting in an 83% PSC prestretch. The different LoPs are summarized in Table 1.

Table 1. Overview of the Different Prestretch Levels Applied in this Study (LoP = Level of Prestretch)

prestretch	normal LoP (%)	increased LoP (%)
biaxial	37.5	57.5
uniaxial under PSCs	57.5	83

The prestretched membranes held by the metal frame are coated in a sputter process. Prior to the process, the membranes are cleaned with deionized air, but no other pretreatment is applied. A mirror-like surface is obtained after the deposition, changing into an out-of-plane buckling or wrinkled surface when the prestretch is released and the membrane is allowed to relax. For PSC prestretched membranes, a well-aligned wrinkle structure is obtained after relaxation, whereas randomly oriented wrinkles are received for biaxially prestretched silicones (compare the right hand side of Figure 1). The entire process is carried out manually.

A vacuum chamber (company CCR) with a dimension of 45 × 45 × 45 cm^3, equipped with two circular 12,7 cm magnetron heads, is used for the deposition process. One head carries a nickel target and the other a graphite (carbon) target. A direct current (DC) sputter generator, used to drive the targets at a constant power of 300 W, is connected to the targets. The targets are located 4.5 cm above a movable specimen carrier. To avoid the condensation of moisture, the vacuum chamber is vented with nitrogen after every process, because the chamber has no load lock.

At the beginning of the process, the vacuum chamber is evacuated by means of a turbo molecular pump (1000 l/s) to a background pressure smaller than 10^{-5} mbar. Then, three pump−purge cycles with argon (purity 99.999%) at a pressure of 10^{-1} mbar are carried out to ensure a clean sputter environment. Afterward, a constant process pressure is obtained by introducing a constant argon gas flow of 15 sccm, and by controlling the desired pressure with a downstream throttle valve. Carbon is sputtered at 1.5 μbar, and nickel at 18.0 μbar, respectively, if only one side of the silicone membrane is coated. If both sides need to be coated subsequently, nickel layers are deposited at a lower process pressure of 1.5 μbar. The above given pressure levels result from preliminary tests on glass slides. Because carbon layers have a higher conductivity at low sputter pressure, we selected a value of 1.5 μbar. A relatively high pressure was chosen for nickel, because of its excellent adhesion on glass slides. Therefore, in the early stage, a high process pressure for Ni and a low process pressure for C were chosen. After finishing all processes on elastomer membranes coated on just one side, problems due to crack formation occurred if the membranes were coated on both sides. This problem could be overcome by developing a nickel layer with reduced residual stress requiring lower process pressures.[45] It turned out that the adhesion of Ni layers to the elastomer is very satisfactory at both process pressures.

When the sputter process is started, the respective target is presputtered for 1.5 min. During the presputtering, the sample is located outside the area of influence of the target. After the presputtering, the sample is moved under the target for the specified process time, and then removed again. When a sandwich layer is desired, the same procedure is subsequently repeated with the second target. Overall, three different types of layers are investigated in this study: a sole nickel electrode with a thickness of 10 nm, a Ni + C sandwich electrode, and a C + Ni sandwich electrode with an overall thickness of 20 nm, respectively (see Table 2).

A cross-shaped pattern of the thin films is realized with a mask process. The shadow mask is fixed on a second metal rack, and placed on the prestretched membrane before deposition. The mask is rotated

https://doi.org/10.1021/acsami.1c10686
ACS Appl. Mater. Interfaces 2021, 13, 39894−39904

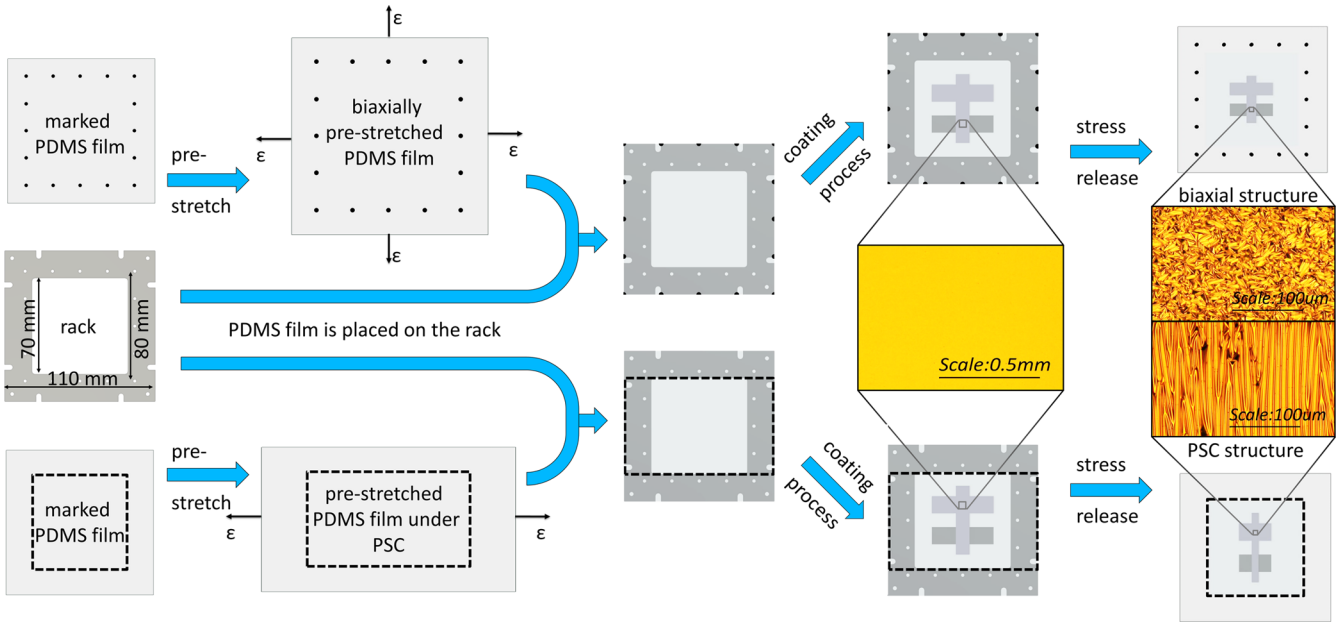

Figure 1. Sample preparation and process steps: either biaxially or under PSCs prestretched silicone membranes are fixed on a metal frame and then sputter coated. Differently wrinkled electrodes are obtained when the membrane is allowed to relax after the sputter coating. The optical microscopy pictures of the electrodes reveal nickel thin films in the flat mirror-like prestretched state and after relaxation of the membranes, respectively. Pictures are obtained with an Olympus BX41 optical light microscope. Reproduced with permission from ref 42. Copyright 2020 Elsevier.

Table 2. Layer Systems of Three Different Types with Their Corresponding Sputter Times[a]

layer abbreviation	first layer	second layer	sputter time Ni [sec]	sputter time C [sec]
C+Ni	C 10 nm	Ni 10 nm	5	60
Ni+C	Ni 10 nm	C 10 nm	5	60
Ni	Ni 10 nm	-	5	-

[a]The colors match the ones of the following result graphs.

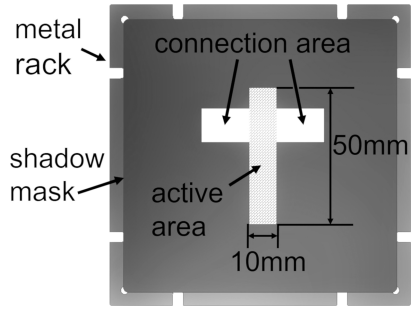

Figure 2. Position and dimensions of the shadow mask. A cross-shaped thin film pattern is created. The membrane is coated on both sides, with the cross-shaped mask being rotated by 180° on the backside. Hence, the overlapping vertical cross bar represents the active area, whereas the vertical one serves as the connection area. Reproduced with permission from ref 42. Copyright 2020 Elsevier.

by 180° when a thin film is also deposited on the backside. The vertical cross bar constitutes the active area, while the horizontal bar serves as the area for the electrical connections (see Figure 2). This electrode geometry is used for all experiments in this study, unless otherwise specified. For more details about the process steps, the reader may refer to ref 41.

Thickness Measurement, Adhesion, and Scanning Electron Microscopy. The thicknesses of the deposited thin films are measured tactilely by means of a Dektak 150 Profilometer indirectly on glass slides, because the sticky and soft surface of silicone does not allow a direct tactile measurement on the membranes. A cover glass is placed in the middle of a glass slide. Then, the glasses are coated up to 300 s with a nickel thin film sputtered at either 1.5 or 18 μbar, respectively, or a carbon thin film. The same sputter parameters used for manufacturing the thin film electrodes on the silicone are applied also in this case. After the coating, the cover glass is removed and the step with the height of the thin film is measured, both for ascending and descending cases. The film thickness is correlated with the sputter time, and hence the deposition rates of the thin films are calculated.

The adhesion of the thin film is investigated by a simple peel-off test. The elastomeric membrane is prestretched on an O-ring, and then sputter coated. Afterward, an adhesive tape is pressed on the deposited surface. When the tape is removed, the adhesion of the deposited thin film can be qualitatively estimated by the out-of-plane deflection of the membrane. Checking for remnants of the thin film on the tape after the peel-off test gives also hints whether delamination occurs.

The wrinkled surfaces of all electrode configurations are analyzed after relaxation by means of a JEOL JSM 6460LV scanning electron microscope (SEM). The secondary electron pictures are recorded with an acceleration voltage of 10 kV and a magnification of 1500.

Resistance and Capacitance versus Strain Measurements. The resistance of the thin film electrodes as a function of strain is investigated on one-side-coated membranes, by means of a self-assembled tensile tester. A LabView program controls uniaxial tensile tests and creep and cycling measurements with and without high voltage applied while simultaneously recording the force, displacement, resistance, and capacitance. The resistance and the capacitance are recorded by means of a Hameg HM 8118 LCR-meter (for further details, see ref 46). At least four single specimens of each type of electrode, that is, Ni, Ni + C, or C + Ni, are tested in a pure shear uniaxial tensile test. A length to width ratio of 5/1, with the pulling direction being perpendicular (see Figure 3) to the long side, allows us to interpret the uniaxial tensile test as a pure shear tensile test.[47,48]

https://doi.org/10.1021/acsami.1c10686
ACS Appl. Mater. Interfaces 2021, 13, 39894−39904

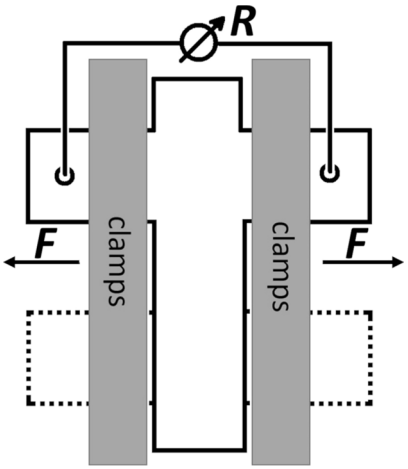

Figure 3. Schematic illustration of the tensile test setup. The cross-shaped electrode is clamped parallel to the vertical crossbar and stretched in the horizontal direction. Here, the resistance of the top electrode is measured. The dashed line represents the electrode deposited on the backside of the sample. By connecting the top electrode with the bottom electrode, the capacitance can be measured as well. Reproduced with permission from ref 42. Copyright 2020 Elsevier.

The pure shear tensile test is carried out with electrodes prestretched under normal conditions, that is, 37.5% biaxially and 57.5% PSC, and with electrodes of the increased level of prestretch (57.5% biaxial and 83% PSC). Every strain level is kept constant for 25 s, while the corresponding resistance is averaged and subsequently plotted versus strain. Starting with a test strain of 0%, this quantity is stepwise increased by 5% with a complete strain relief between the steps. Two smaller steps of 2.5% are added directly around the LoP. For specimens with the increased LoP, the lower strain levels are increased stepwise by 10% until the LoP is reached. Above the LoP, the 5% increment is executed again.

For capacitance measurements, the same tensile tester is used, and the same testing procedure is applied with membranes coated on both sides. Therefore, nickel electrodes manufactured at low process pressure are tested. Only electrodes deposited on membranes with normal LoP are analyzed.

Fatigue Test. The resistance as a function of strain is also measured in a fatigue test. For this investigation, 10 million sinusoidal cycles of mechanical stretching are performed at a frequency of 20 Hz, by means of a Bose ElectroForce 3230 material testing machine. Prestretched membranes with all types of electrodes are tested. 37.5% biaxially prestretched membranes are tested at strain levels of both 35 and 50%, while 57.5% PSC prestretched membranes are tested by applying 55 and 65% of test strain.

Force versus Strain Measurements with High Voltage. Force−strain characteristics are evaluated by means of a tensile tester, performed with and without high voltage applied to the DE samples. Five repetitive cycles of strain are performed with a strain rate of 10%/s, out of which the fourth cycle is analyzed to avoid misleading interpretations, because the viscoelastic characteristics, such as the hysteresis and the force change drastically in the first two cycles due to the Mullin's effect. At first, five cycles without voltage are carried out, followed by five cycles with 3 kV. Membranes with normal LoP are investigated in this test. The 37.5% biaxially prestretched membranes are cycled from 0 to 50%, while 57.5% PSC prestretched membranes are tested in between 0 and 70%, respectively. For this purpose, the same tensile test setup is used again.[46] All types of electrodes are tested, that is, Ni, Ni + C, and C + Ni. Because both side-coated membranes are required for these experiments, nickel electrodes deposited at low process pressures are utilized.

RESULTS AND DISCUSSION

Thickness Measurement and Adhesion. For carbon, a deposition rate of 0.16 ± 0.01 nm/s is measured, while the rate of nickel is determined at two different sputter pressures, that is, 2.36 ± 0,25 nm/s at 1.5 μbar and 2.52 ± 0,4 nm/s at 18 μbar, respectively. Hence, a 10 nm carbon film is generated in about 1 min, while 5 s are sufficient to deposit 10 nm of Ni. Differences between specified and calculated thicknesses originate from the manually performed sputter process. Within the 5 s, the specimen is manually rotated under the target, coated, and then rotated out again. Hence, the exact coating time and thus the exact thickness of the thin film could vary slightly for every process (for details, see ref 41). The authors specify the thickness of the thin films as 10 nm to provide an appropriate classification.

A large deflection of the coated membrane during the peel-off test confirms a good adhesion between the thin film and the silicone (see Figure 4). No delamination occurs and after

Figure 4. Adhesion is proved with a peel-off test. An adhesive tape is stuck onto the coated membrane and then peeled off again. The peel-off force is transferred via the thin film electrode to the silicone resulting in an out of plane deformation of the membrane. No delamination of the thin film occurs. The removed tape is free from remnants, confirming a good adhesion between the thin film electrode and the silicone membrane. This test was performed with all electrode configurations.

removing the tape, no remnants remain on the tape. This test was conducted with all three electrode configurations directly after the manufacturing. Two months later the test was repeated, and the same results were obtained. No aging effect of the adhesion could be manifested by the peel-off test. At strain levels around 200%, applied during the tensile tests, also no mechanical degradation or delamination of the thin film was observed.

In Figure 5, the wrinkle structures of the respective electrode configurations are depicted after relaxation. The first row shows previously biaxially prestretched membranes, while the second row displaces the PSC prestretched membranes. All pictures are taken with the same magnification, and thus are easy to compare. When the membrane was biaxially prestretched, a random wrinkle orientation results after relaxation. Otherwise, a well-aligned and preferentially horizontally oriented wrinkle structure is revealed, because the PSC prestretch was oriented in the vertical direction. Clearly, the wrinkle structure gets finer from the left to the right, that is, from C + Ni over N + C to the finest structure of Ni.

Resistance versus Strain Measurements. Figure 6 depicts the results of the uniaxial resistance measurements of

https://doi.org/10.1021/acsami.1c10686
ACS Appl. Mater. Interfaces 2021, 13, 39894−39904

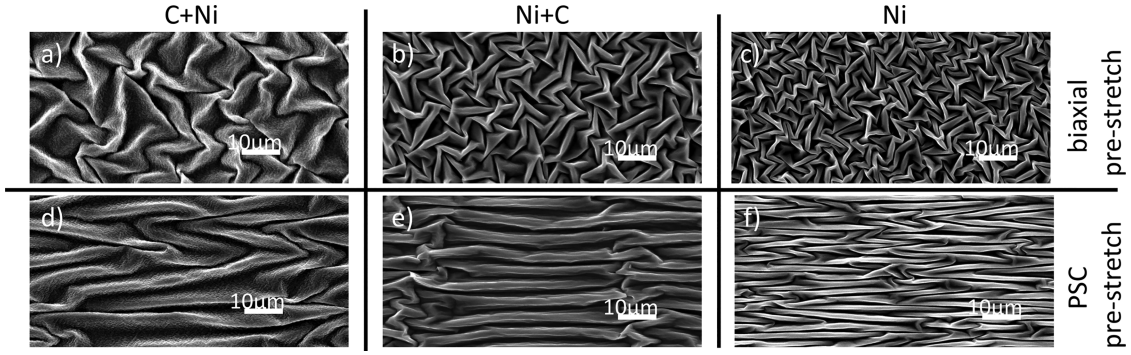

Figure 5. SEM images in the relaxed state of all electrode configurations, all with the same magnification of 1500. In the first row (a–c), the biaxially prestretched membranes are shown. PSC prestretched membranes are placed in the second row (d–f). The wrinkle structure becomes finer from the left to the right, hence from C + Ni (a,d) over Ni + C (b,e) to Ni (c,f) thin films. Enlarged pictures can be found online (Supporting Information).

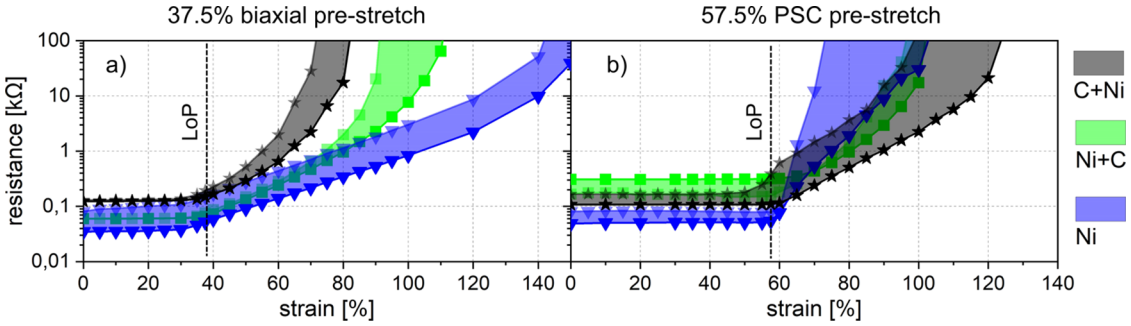

Figure 6. Resistance vs strain results for Ni + C (green), Ni (blue), and C + Ni (grey) electrodes are shown. Part (a) presents the results of biaxially prestretched membranes, whereas PSC prestretched membranes are shown in the plot (b). On previously biaxially prestretched membranes, Ni electrodes can be stretched up to 140% before the resistance passes 10 kΩ, whereas C + Ni electrodes exceed this value already at 70%. On PSC prestretched membranes, the characteristic is changed. Here, the 10 kΩ value of Ni electrodes is located at lower strain levels compared to the Ni + C and the C + Ni electrodes. Hence, the resistance at high strain levels is dependent on both, the electrode configuration and the prestretch as well.

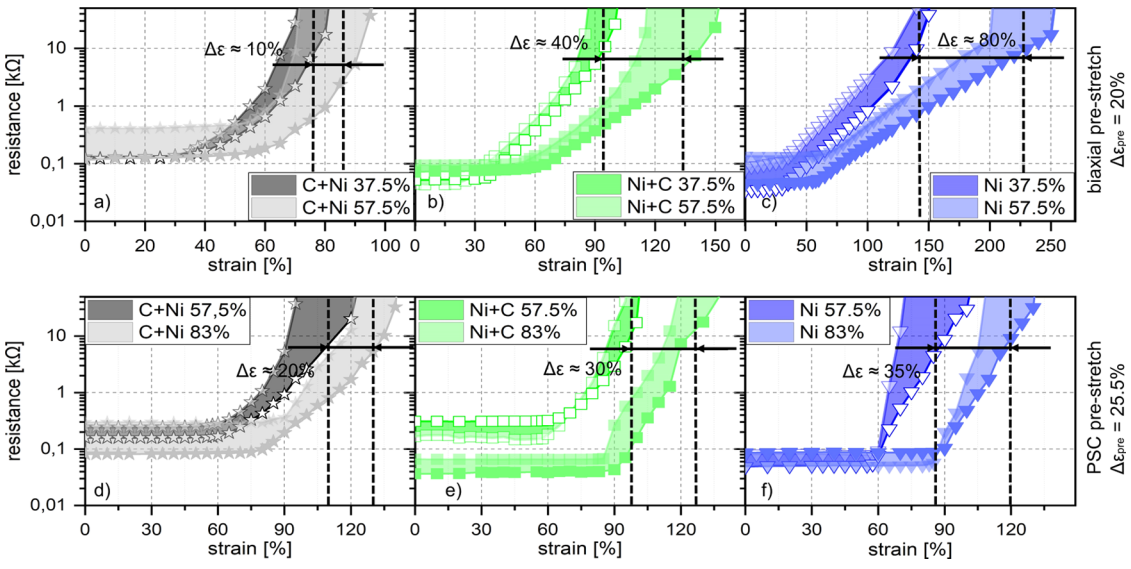

Figure 7. Resistance vs strain plots for different LoP. The results of electrodes deposited onto membranes with normal prestretch are compared to electrodes deposited onto membranes with increased prestretch. In the first row (a–c), biaxially prestretched membranes are shown, while PSC prestretched membranes are plotted in the 2nd row (d–f). Note: the *x*-axes have different scales. For biaxially prestretched membranes, a 20% LOP-increase yields more stretchability of 10, 40%, and even 80% for C + Ni, Ni + C, and Ni electrodes, respectively. For PSC prestretched membranes, a 25.5% LOP-increase entails an improvement of stretchability of 20% for C + Ni, 30% for Ni + C, and 35% for Ni electrodes.

both biaxially prestretched (a) and PSC prestretched membranes (b). Each type of electrode is plotted as a colored

https://doi.org/10.1021/acsami.1c10686
ACS Appl. Mater. Interfaces 2021, 13, 39894–39904

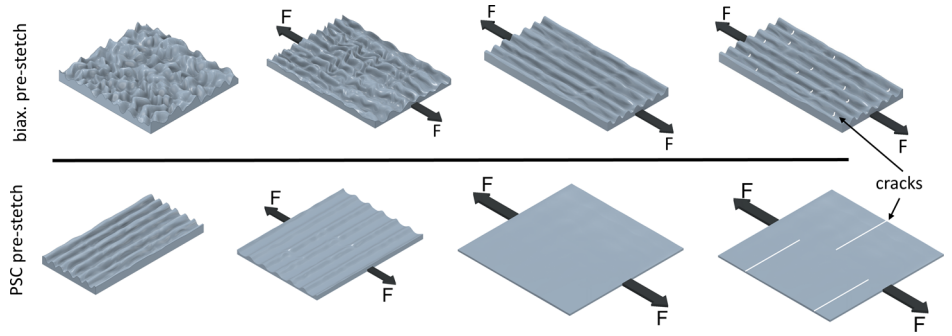

Figure 8. Illustration of the unfolding process of coated biaxially and PSC prestretched membranes, during an uniaxial tensile test with the force F. A partially wavy structure with a rather huge number of small cracks remains for biaxially prestretched membranes. In contrast, few but large cracks propagate through a nearly flat metal electrode if a PSC prestretched membrane is strained uniaxially. In the latter case, the crack-induced resistance increase occurs at lower strains.

area, whereas the maximum and the minimum values of at least four samples of every electrode type limit the respective colored area.

Some interesting conclusions can be drawn from the graphs. Up to the LoP, the resistance of the thin film electrodes remains constant at approx. 100 Ω/square. When the LoP is reached, a section with a linear slope occurs. Depending on the electrode and prestretch configuration, the linear ranges extend over different strain ranges. Then, the slopes of the curves increase further, eventually leading to the electrical failure (in this paper defined as 100 kΩ/square). On biaxially prestretched membranes (Figure 6a), the resistance exceeds the 100 kΩ/square at a strain of approximately 70% for C + Ni and 90% for Ni + C sandwich films, respectively, while the sole Ni layer remains conductive to strain levels up to 140%. Interestingly, the order of the resistance increase is reversed for the PSC-prestretched membranes (Figure 6b). The sole Ni-layer loses its conductivity first, at approx. 80%, that is, only 20% above the LoP. For the Ni + C layer, 95% is the critical strain value. The best electrode on PSC prestretched membranes is the C + Ni layer with the highest threshold at 120%. These experiments clearly reveal a systematic interplay between the type and level of prestretch and the thin film configuration. In addition to the prestretch, which provides a geometrical buffer thanks to the formation of wrinkles after relaxation, the type of thin film is also crucial for a low resistance at high strain levels. A pure nickel electrode deposited onto biaxially prestretched membranes is favorable, when high strain levels are needed in a pure shear operating mode. On PSC prestretched membranes, a C + Ni electrode represents the best choice, because it remains well conductive to strains of approximately 120%. A further important requirement for excellent conductivity at high strain levels is a good adhesion between silicone and the thin films, as shown for all three film configurations (compare above). A good adhesion avoids delamination, and ensures a homogeneous force transfer from the silicone membrane to the thin film, thus preventing critical local stress concentrations.[49]

In the next step, resistance-strain measurements are performed with an increased level of prestretch, resulting in the plots of Figure 7. The first row (Figure 7a–c) shows biaxially prestretched membranes with different LOPs, whereas the second row (Figure 7d–f) displays PSC prestretched membranes, again with different LOPs. C + Ni (a,d), Ni + C (b,e), and Ni electrodes (c,f) are evaluated. The colored areas again contain at least four specimens, and they are framed by the maximum and the minimum curve. The data for the samples with normal LoP are identical to those ones in Figure 6, but plotted on differently scaled *x*- and *y*-axes. The difference between the normal LoP (37.5%) and the increased LoP (57.5%) for biaxially prestretched membranes is 20%. Interestingly, the resistance increase is strongly dependent on the type of electrode. This 20% increase of the biaxial prestretch level shifts the degradation of the Ni electrode by 80% to strains of up to approximately 225%. Smaller improvements of 40 and 10% are achieved for Ni + C and C + Ni electrodes, respectively. This may be due to the fact that the silicone membrane with the thicker 20 nm films of Ni + C and C + Ni, respectively, did not shrink completely to their initial dimensions, as these films offer higher mechanical resistance to the relaxation process. This could be verified by thickness measurements of relaxed membranes with a dial gauge. The thickness of uncoated membranes was compared to membranes coated on both sides. The coated DEs are thinner than the uncoated ones. The membrane with the C + Ni electrode is the thinnest membrane, followed by the Ni + C and the Ni coated membrane, respectively. Due to the volume being constant, a thinner membrane is equivalent to a more elongated membrane, and hence to a not fully relaxed membrane. Thus, the above measured order of resistance increase becomes plausible. Measuring an elastomeric membrane with a spring-loaded dial gauge involves some unspecified uncertainties. Therefore, absolute values are not given here but the trends were obvious and reproducible. The SEM analysis of Figure 5 also provides evidence for this interpretation. Because the nickel thin film hinders relaxation the least, the silicone membrane forms a finer Ni wrinkle structure than a Ni + C or a C + Ni wrinkle structure.

In the case of 25.5% augmented PSC prestretched membranes, the Ni and the Ni + C electrodes exhibit an increased stretchability of only 35 and 30%, respectively. Again, the smaller improvement of the Ni + C electrode is attributed to a higher mechanical resistance against wrinkle formation of the 20 nm film compared to the thinner Ni film, meaning that the prestretched membrane would not completely relax. For the experimental characterization in the tensile test, the silicone membrane is always assumed to be completely relaxed. Hence, the clamped tensile test specimen at 0% nominal test strain is already prestrained with a small undefined intrinsic strain. Thus, the measured electrode would be flattened already at lower test strain levels. Hence, the mechanical precondition for holding the low electrical resistance at high strain levels is

https://doi.org/10.1021/acsami.1c10686
ACS Appl. Mater. Interfaces 2021, 13, 39894–39904

reduced. With carbon as a sublayer of the C + Ni configuration, the increased prestretch levels lead to a low performance enhancement, smaller than the change of the LoPs. This corresponds to the finding that the C + Ni electrode works most effectively against the relaxation of the silicone membrane. With a higher LoP, this effect becomes more visible.

The wrinkled structure seems to be a key feature for maintaining low resistance at high strain levels. In this way, the limited elasticity of metals of a few percent can be bypassed. At strain levels below the LoP, the wrinkles get merely unfolded, hence no resistance increase is noticeable. Above the LoP, the thin film electrode itself is stressed, that is, cracks may occur and the resistance starts to increase (see Figure 8). The effect that a prestretch is beneficial for obtaining stretchable and flexible electrodes was already confirmed by other groups.[28,37,50−54] When a biaxially prestretched membrane with a randomly oriented wrinkled structure is elongated in a pure shear tensile test, a surface with an inhomogeneous stress distribution is received. Wrinkles oriented perpendicular to the tensile direction are flattened, but a wavy structure parallel to the applied strain remains. Therefore, occurring cracks cannot propagate the whole surface. They are stopped due to the inhomogeneous stress distribution on the wavy surface. In this case, the local stresses can be reduced by twists and deflections around the opening cracks.[50,55] As a result, the electrode may have a large number of small cracks. Very importantly, a lot of still connected conductive paths are maintained, thus ensuring the low resistance (cf. Figure 8 1st row). On PSC prestretched membranes, an electrode with a well-aligned wrinkle structure can be unfolded to a nearly ideal flat surface during tensile testing. Thus, no obstacles for crack propagation are available, and hence few but long cracks will lead to a complete transection of the thin film. This failure of the electrodes occurs at lower strain levels above the LoP, compared to electrodes deposited onto biaxially prestretched membranes (compare Figure 8 2nd row).

The possibility to adapt the thin film configuration to the type and the level of prestretch, in order to maintain conductive electrodes even at high strain levels, is a highly desirable feature. All prepared electrode configurations with higher LoPs shift the threshold of resistance increase toward higher strain levels. A 57.5% biaxially prestretched membrane equipped with a 10 nm sole Ni-electrode remains at low resistance up to 200% of pure shear strain, as shown in Figure 7b.

Capacitance versus Strain Measurements. Capacitance−strain measurements of all thin film configurations, deposited either onto 37.5% biaxially or onto 57.5% PSC prestretched membranes, are depicted in Figure 9a,b respectively. The capacitances are approximately linearly dependent on the strain below the LoP. Only the sole Ni electrode on PSC membranes exhibits a decrease of the capacitance just below the LoP. The PSC prestretched slopes (b) are higher compared to the biaxially prestretched capacitors. This may be due to the complete unfolding of the aligned wrinkle structure in the PSC case, whereas the randomly oriented wrinkles, on the other hand, are only partially flattened during the tensile test. The latter case does not lead to a complete unfolding of the sandwich (compare Figure 8) and hence lower capacitance results. The curves of the different layers of one prestretched type are almost parallel, whereby the capacitance of the C + Ni electrodes is higher

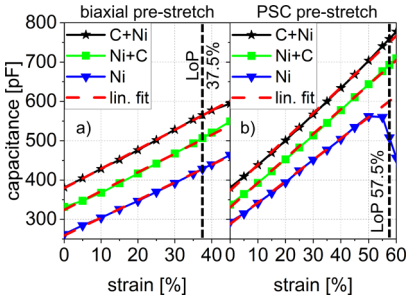

Figure 9. Capacitance vs tensile strain measurements for 37.5% biaxially (a) and 57.5% PSC prestretched (b) samples with the respective linear fits (red-dotted lines). The capacitance is linearly dependent on the strain below the LoP. For a certain type of prestretch, the curves are almost parallel. The highest capacitance is observed for C + Ni electrodes and the lowest one for Ni electrodes.

compared to Ni + C and Ni electrodes, respectively. The most striking effect of the capacities of Figure 9 is the systematically different initial value of about 40%. This is remarkable because a 10 or 20 nm thin metal layer on a 50 μm thick polymer can induce such drastically different capacitances. However, as already stated above, the electrode-dependent initial capacitance is connected to the degree of relaxation at zero strain. If the membrane is still slightly elongated, the capacitor area is increased while the distance between the electrodes is decreased, both of which contribute to a higher initial capacitance. Because the C + Ni electrode exhibits the highest mechanical resistance against the relaxation, such DEs reveal the largest initial capacitance. The deformation of the capacitors geometry during the tensile test is equal for all kinds of thin films on a certain prestretch configuration. Therefore, the slopes of the capacitance curves are parallel. A linear dependency of the capacitance versus strain was also demonstrated by Benslimane et al.,[56] by measuring the capacitance of corrugated DE-membranes coated with thin conducting films. The linear dependence of capacitance is advantageous for mechanical sensors, for example, displacement or distance sensors. For applications with strain levels below the LOP, the linear capacitance of the metallic wrinkled electrodes can be used to develop capacitive sensors. If both the capacitance as well as the resistance of such coated membranes are measured and evaluated with a suitable sensor electronic, the measuring range may be extended to the whole range of strain as shown in the capacitance plot (Figure 9) and the resistance plots of Figures 6 and 7.

Fatigue Test. The long-term stability of all electrode configurations deposited on either PSC or biaxially prestretched membranes was proved by means of fatigue tests with 10 million cycles. For both LoPs, fatigue strain levels directly below and above the LoP were chosen. The 37.5% biaxially prestretched membranes were tested up to 50% of strain, whereas for the 57.5% PSC prestretched membranes, a maximum of 65% strain was chosen. The deposited electrodes on PSC prestretched membranes are more vulnerable to degradation if the LoP is exceeded. In both cases, the resistance remains almost constant at low values of approx. 500 Ω/square, when the test strain is kept below the respective LoP. A test strain higher than the LoP causes the electrodes to degrade slightly. However, all electrode configurations end up with resistances below 5 kΩ/square, after 10 million cycles of mechanical load. (for the graphs, see Supporting Information, available online).

https://doi.org/10.1021/acsami.1c10686
ACS Appl. Mater. Interfaces 2021, 13, 39894−39904

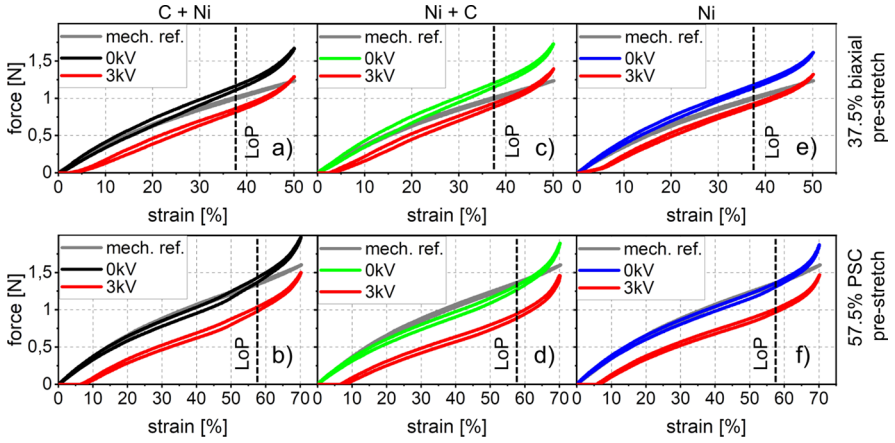

Figure 10. Force−strain measurements with and without applied voltage of the C + Ni (a,b), the Ni + C (c,d), and the Ni electrodes (e,f) on either 37.5% biaxially prestretched (a,c,e) and on PSC prestretched membranes (b,d,f). The mechanical reference—a membrane without electrodes—is shown in the graphs (gray curves) for comparison. When a voltage is applied, a force-drop (red curves) is recognizable for all electrode and prestretch configurations. The membrane is then elongated due to the attraction of the oppositely charged electrodes, and hence less force is needed to stretch the membrane to a certain strain level.

Force versus Strain Measurements with and without High Voltage. In Figure 10, the force characteristics of membranes without and with high voltage applied (red curves) are compared for the different thin film configurations. The first row shows biaxially prestretched membranes (a,c,e), while PSC prestretched membranes are plotted in the second row (b,d,f). In every plot, the characterization of a membrane without any thin film is shown as the mechanical reference. The force needed to elongate the both side coated membranes to a certain strain level is lower if a voltage of 3 kV is applied because the voltage causes an attraction of the electrodes, squeezing and expanding the membrane in between. Hence, the force response decreases with applied voltage. This response is valid for all film configurations of Figure 10.

The details of these measurements are discussed as follows. Below the LOPs, all zero voltage curves are very close to the mechanical reference, being a silicone membrane without any layer. At about the LOPs, all curves begin to deviate from the reference, their slopes increase strongly. This clearly coincides with the unfolding of the metallic layers as illustrated in Figure 8. From then on, the electrodes have a significant influence on the mechanical stiffness of the DE-membrane due to the high Young's modulus of metals. A detailed look on the force response of the PSC prestretched DEs shows the coated DE a little bit below the mechanical reference as long as the LOP is not exceeded. The wrinkles are under compression and hence help to unfold and reduce the necessary elongation force until the surface is flat.

In the biaxially prestretched case, a stiffening of the membrane due to the metallic electrodes is observable over the complete strain range. The compressed and randomly oriented wrinkle structure only partially supports the uniaxial elongation. In addition, a rearrangement of the wrinkle structure and the working against notadvantageously oriented wrinkles during the elongation result in a mechanical reinforcement of the coated DE.

Comparable results were obtained by Benslimane et al. as well. When the geometrical buffer of their corrugated surface was consumed, the load to reach a certain deformation increases excessively.[56] Such corrugated surfaces provide extremely anisotropic electromechanical properties. Our biaxially prestretched membranes are superior, with respect to this point. Pimpin et al. were working on structured metal electrodes on not prestretched membranes. They report a coverage-dependent performance. The flat metal surface stiffens the dielectric in their study. No wrinkles were available.[33] In our case, the stiffening of the membranes due to the wrinkled metal electrodes is negligible as long as the LoP is not exceeded. The high-voltage measurements, which reveal a force difference compared to the zero voltage case, confirm that the metallic electrode can be used as an active DE-electrode material. This force difference is the basis for designing biasing mechanisms for highly efficient actuator systems.[57−60] The performance of an actuator suffers from its energetic losses per cycle, shown in Figure 10 as hysteresis. Despite the hysteresis, the force gap is big enough in our case. Based on simulations in order to develop an appropriate biasing mechanism,[61] Neu et al. already presented a working circular actuator concept applying a wrinkled Ni-based electrode.[58] Furthermore, these measurements prove that the dielectric strength of the Elastosil membrane is not reduced by the sputtering process. Because the tensile test is considered to be a pure shear test, a strain of 70% causes a thickness reduction of approximately 40%. Thus, a 30 μm thick silicone membrane withstands 3 kV. This corresponds to a dielectric strength of 100 V/μm, a value in accordance with the datasheet.

CONCLUSIONS AND OUTLOOK

The highly remarkable electromechanical properties, such as an extremely high stretchability of up to 200% of strain, can be explained and correlated with the wrinkled electrodes and hence to the type of prestretch as well as to the electrode material itself. The presented thin film electrodes are regarded as a complementary alternative to CB electrodes. With a resistance 2 orders of magnitude lower than that of the usually applied CB electrodes, combined with a linear dependency of the capacitance on strain, the Ni-based electrode is best suited for DE capacitive sensors. Additionally, it is a highly compliant electrode with a reliable fatigue behavior, even after 10 million cycles. The system remains highly conductive even at high strain levels. With 57.5% of biaxial prestretch, approx. 200% of strain can be applied before a pure Ni electrode loses its

https://doi.org/10.1021/acsami.1c10686
ACS Appl. Mater. Interfaces 2021, 13, 39894−39904

conductivity. These results, together with the high voltage measurements, prove that the electrodes are advantageous for high-frequency or high-efficiency DE applications. In order to achieve the best possible performance of the DE system, the type of prestretch, in conjunction with the corresponding thin film configuration, can be adapted to the respective application. Of course, a further property optimization regarding thin film parameters, such as thickness and deposition temperature among others, is expected.

In future research, we will further pursue our aim of cooperation, that is, the development of an array of cooperatively working microactuators and sensors based on DE-technology. For such miniaturized applications, the pattern definition of the electrode should no longer be realized by a mask process, especially for high-volume production. A laser structuring process used to define the electrode geometry, as well as the electrical supply lines on a completely coated film, is currently under development. An automated foil stretcher is also under construction, to replace the manual process of prestretching to more reproducible predefined values. We are confident to establish a DE— electrode system for multiple applications.

■ ASSOCIATED CONTENT

Supporting Information

The Supporting Information is available free of charge at https://pubs.acs.org/doi/10.1021/acsami.1c10686.

Tensile test (MP4)

Applying a high voltage (MP4)

Results of the fatigue tests of all electrode configurations and SEM pictures of the PSC prestretched Ni thin film electrode, PSC prestretched Ni + C thin film electrode, PSC prestretched C + Ni thin film electrode, biaxially prestretched Ni thin film electrode, biaxially prestretched Ni + C thin film electrode, and biaxially prestretched C + Ni thin film electrode (PDF)

■ AUTHOR INFORMATION

Corresponding Author

Jonas Hubertus − *Sensors and Thin Film Group, University of Applied Sciences, Saarbrücken 66117, Germany;* orcid.org/0000-0001-9388-0454; Phone: +49 681 85787 651; Email: jonas.hubertus@htwsaar.de

Authors

Julian Neu − *Department of Systems Engineering, Department of Materials Science & Engineering, Saarland University, Saarbrücken 66123, Germany*

Sipontina Croce − *Department of Systems Engineering, Department of Materials Science & Engineering, Saarland University, Saarbrücken 66123, Germany*

Gianluca Rizzello − *Department of Systems Engineering, Department of Materials Science & Engineering, Saarland University, Saarbrücken 66123, Germany*

Stefan Seelecke − *Department of Systems Engineering, Department of Materials Science & Engineering, Saarland University, Saarbrücken 66123, Germany*

Günter Schultes − *Sensors and Thin Film Group, University of Applied Sciences, Saarbrücken 66117, Germany*

Complete contact information is available at: https://pubs.acs.org/10.1021/acsami.1c10686

Author Contributions

The manuscript was written with contributions of all authors. All authors have given approval to the final version of the manuscript.

Funding

The project with the title "DECMAS—DE Membranes for Cooperative Micro-Actuator and Sensor Concepts" (Projects: RI3030/2-1, SCHU1609/7-1, and SE704/9-1) is gratefully funded by the German Research Foundation DFG, and is part of DFG priority program SPP 2206 "KOMMMA—Cooperative Multistage Multistable Micro Actuator Systems".

Notes

The authors declare no competing financial interest.

■ ACKNOWLEDGMENTS

We gratefully acknowledge the support from the whole Sensors and Thin Film Group, especially the support from our student assistant Simon Kraß and the great cooperation from our project partners. The authors also thank Dr. Olivia Freitag-Weber for taking the SEM pictures.

■ ABBREVIATIONS

C, chemical element carbon
CB, carbon black
Cr, chemical element chromium
DC, direct current
DE, dielectric elastomer
LoP, level of prestretch
Ni, chemical element nickel
PSC, pure shear conditions
SEM, scanning electron microscope

■ REFERENCES

(1) Carpi, F.; de Rossi, D.; Kornbluh, R.; Pelrine, R. E.; Sommer-Larsen, P. *Dielectric Elastomers as Electromechanical Transducers:Fundamentals, Materials, Devices, Models and Applications of an Emerging Electroactive Polymer Technology*; Elsevier, 2008.

(2) Pelrine, R.; Kornbluh, R.; Joseph, J.; Heydt, R.; Pei, Q.; Chiba, S. High-Field Deformation of Elastomeric Dielectrics for Actuators. *Mater. Sci. Eng. C* **2000**, *11*, 89−100.

(3) Rustighi, E.; Kaal, W.; Herold, S.; Kubbara, A. Experimental Characterisation of a Flat Dielectric Elastomer Loudspeaker. *Actuators* **2018**, *7*, 28.

(4) Hosoya, N.; Masuda, H.; Maeda, S. Balloon Dielectric Elastomer Actuator Speaker. *Appl. Acoust.* **2019**, *148*, 238−245.

(5) Carpi, F.; Frediani, G.; Turco, S.; De Rossi, D. Bioinspired Tunable Lens with Muscle-Like Electroactive Elastomers. *Adv. Funct. Mater.* **2011**, *21*, 4152−4158.

(6) Shian, S.; Diebold, R. M.; Clarke, D. R. Tunable Lenses Using Transparent Dielectric Elastomer. *Actuators. Opt. Express* **2013**, *21*, 8669−8676.

(7) Anderson, I. A.; Gisby, T. A.; McKay, T. G.; O'Brien, B. M.; Calius, E. P. Multi-Functional Dielectric Elastomer Artificial Muscles for Soft and Smart Machines. *J. Appl. Phys.* **2012**, *112*, 041101.

(8) Chen, Y.; Zhao, H.; Mao, J.; Chirarattananon, P.; Helbling, E. F.; Hyun, N.-S. P.; Clarke, D. R.; Wood, R. J. Controlled Flight of a Microrobot Powered by Soft Artificial Muscles. *Nature* **2019**, *575*, 324−329.

(9) Boys, H.; Frediani, G.; Poslad, S.; Busfield, J.; Carpi, F. A Dielectric Elastomer Actuator-Based Tactile Display for Multiple Fingertip Interaction with Virtual Soft Bodies. In *Electroactive Polymer Actuators and Devices (EAPAD) 2017*; Bar-Cohen, Y., Ed.; SPIE, 2017; Vol. *101632D*.

(10) Vertechy, R.; Fontana, M.; Rosati Papini, G. P.; Forehand, D. In-Tank Tests of a Dielectric Elastomer Generator for Wave Energy

Harvesting. In *Electroactive Polymer Actuators and Devices (EAPAD) 2014*; Bar-Cohen, Y., Ed.; SPIE, 2014; Vol. *90561G*.
(11) Moretti, G.; Righi, M.; Vertechy, R.; Fontana, M. Fabrication and Test of an Inflated Circular Diaphragm Dielectric Elastomer Generator Based on PDMS Rubber Composite. *Polymers* **2017**, *9*, 283.
(12) Jean-Mistral, C.; Jacquet-Richardet, G.; Sylvestre, A. Parameters Influencing Fatigue Life Prediction of Dielectric Elastomer Generators. *Polym. Test.* **2020**, *81*, 106198.
(13) Böse, H.; Ocak, D.; Ehrlich, J. Applications of Pressure-Sensitive Dielectric Elastomer Sensors. In *Electroactive Polymer Actuators and Devices (EAPAD) 2016*; Bar-Cohen, Y., Vidal, F., Eds.; SPIE, 2016; Vol. *97982C*.
(14) Huang, B.; Li, M.; Mei, T.; McCoul, D.; Qin, S.; Zhao, Z.; Zhao, J. Wearable Stretch Sensors for Motion Measurement of the Wrist Joint Based on Dielectric Elastomers. *Sensors* **2017**, *17* (). DOI: DOI: 10.3390/s17122708.
(15) Loew, P.; Rizzello, G.; Seelecke, S. Pressure Monitoring Inside a Polymer Tube Based on a Dielectric Elastomer Membrane Sensor. In *Electroactive Polymer Actuators and Devices (EAPAD) XX*; Bar-Cohen, Y., Ed.; SPIE, 2018; p 53.
(16) Ni, N.; Zhang, L. Dielectric Elastomer Sensors. In *Elastomers*; Cankaya, N., Ed.; InTech, 2017.
(17) Rosset, S.; Shea, H. R. Flexible and Stretchable Electrodes for Dielectric Elastomer Actuators. *Appl. Phys. A* **2013**, *110*, 281−307.
(18) Watanabe, M.; Shirai, H.; Hirai, T. Wrinkled Polypyrrole Electrode for Electroactive Polymer Actuators. *J. Appl. Phys.* **2002**, *92*, 4631−4637.
(19) Rizzello, G.; Fugaro, F.; Naso, D.; Seelecke, S. Simultaneous Self-Sensing of Displacement and Force for Soft Dielectric Elastomer Actuators. *IEEE Robot. Autom. Lett.* **2018**, *3*, 1230−1236.
(20) Fasolt, B.; Hodgins, M.; Rizzello, G.; Seelecke, S. Effect of Screen Printing Parameters on Sensor and Actuator Performance of Dielectric Elastomer (DE) Membranes. *Sens. Actuators, A* **2017**, *265*, 10−19.
(21) Klug, F.; Solano-Arana, S.; Hoffmann, N. J.; Schlaak, H. F. Multilayer Dielectric Elastomer Tubular Transducers for Soft Robotic Applications. *Smart Mater. Struct.* **2019**, *28*, 104004.
(22) Solano-Arana, S.; Klug, F.; Mößinger, H.; Förster-Zügel, F.; Schlaak, H. F. A Novel Application of Dielectric Stack Actuators: a Pumping Micromixer. *Smart Mater. Struct.* **2018**, *27*, 074008.
(23) Hodgins, M.; Seelecke, S. Systematic Experimental Study of Pure Shear Type Dielectric Elastomer Membranes with Different Electrode and Film Thicknesses. *Smart Mater. Struct.* **2016**, *25*, 095001.
(24) Schlatter, S.; Rosset, S.; Shea, H. Inkjet Printing of Carbon Black Electrodes for Dielectric Elastomer Actuators. In *Electroactive Polymer Actuators and Devices (EAPAD) 2017*; Bar-Cohen, Y., Ed.; SPIE, 2017; p 1016311.
(25) Sarban, R.; Lassen, B.; Willatzen, M. Dynamic Electromechanical Modeling of Dielectric Elastomer Actuators With Metallic Electrodes. *IEEE/ASME Trans. Mechatron.* **2012**, *17*, 960−967.
(26) Brochu, P. Dielectric Elastomers for Actuation and Energy Harvesing, Ph.D. Dissertation, University of California: Los Angeles, 2012, https://escholarship.org/uc/item/7kf261zf#main (accessed 2021-04-22).
(27) Benslimane, M.; Kiil, H.-E.; Tryson, M. J. Electromechanical Properties of Novel Large Strain PolyPower Film and Laminate Components for DEAP Actuator and Sensor Applications. In *Electroactive Polymer Actuators and Devices (EAPAD) 2010*; Bar-Cohen, Y., Ed.; SPIE, 2010; p 764231.
(28) Low, S.-H.; Lau, G.-K. Bi-Axially Crumpled Silver Thin-Film Electrodes for Dielectric Elastomer Actuators. *Smart Mater. Struct.* **2014**, *23*, 125021.
(29) Lacour, S. P.; Wagner, S.; Huang, Z.; Suo, Z. Stretchable Gold Conductors on Elastomeric Substrates. *Appl. Phys. Lett.* **2003**, *82*, 2404−2406.
(30) Ong, H.-Y.; Shrestha, M.; Lau, G.-K. Microscopically Crumpled Indium-Tin-Oxide Thin Films as Compliant Electrodes with Tunable Transmittance. *Appl. Phys. Lett.* **2015**, *107*, 132902.
(31) Verplancke, R.; Bossuyt, F.; Cuypers, D.; Vanfleteren, J. Thin-Film Stretchable Electronics Technology Based on Meandering Interconnections: Fabrication and Mechanical Performance. *J. Micromech. Microeng.* **2012**, *22*, 015002.
(32) Fan, J. A.; Yeo, W.-H.; Su, Y.; Hattori, Y.; Lee, W.; Jung, S.-Y.; Zhang, Y.; Liu, Z.; Cheng, H.; Falgout, L.; Bajema, M.; Coleman, T.; Gregoire, D.; Larsen, R. J.; Huang, Y.; Rogers, J. A. Fractal Design Concepts for Stretchable Electronics. *Nat. Commun.* **2014**, *5*, 3266.
(33) *Micro Electrostrictive Actuator with Metal Compliant Electrodes for Flow Control Applications-17th IEEE International Conference on Micro 2004*; Pimpin, A., Suzuki, Y., Kasagi, N., Eds.; Electro Mechanical Systems, 2004.
(34) Won, P.; Park, J. J.; Lee, T.; Ha, I.; Han, S.; Choi, M.; Lee, J.; Hong, S.; Cho, K.-J.; Ko, S. H. Stretchable and Transparent Kirigami Conductor of Nanowire Percolation Network for Electronic Skin Applications. *Nano Lett.* **2019**, *19*, 6087−6096.
(35) Chen, D.; Liang, J.; Pei, Q. Flexible and Stretchable Electrodes for Next Generation Polymer Eectronics: a Review. *Sci. China Chem.* **2016**, *59*, 659−671.
(36) Lee, P.; Lee, J.; Lee, H.; Yeo, J.; Hong, S.; Nam, K. H.; Lee, D.; Lee, S. S.; Ko, S. H. Highly Stretchable and Highly Conductive Metal Electrode by Very Long Metal Nanowire Percolation Network. *Adv. Mater.* **2012**, *24*, 3326−3332.
(37) Low, S.-H.; Lau, G.-K. The Effect of Folds in Thin Metal Film Electrodes Used in Dielectric Elastomer Actuators. In *Electroactive Polymer Actuators and Devices (EAPAD) 2013*; Bar-Cohen, Y., Ed.; SPIE, 2013; p 86872.
(38) Shrestha, M.; Asundi, A.; Lau, G.-K. Smart Window Based on Electric Unfolding of Microwrinkled TiO 2 Nanometric Films. *ACS Photonics* **2018**, *5*, 3255−3262.
(39) Cheng, T.; Zhang, Y.; Lai, W.-Y.; Huang, W. Stretchable Thin-Film Electrodes for Flexible Electronics with High Deformability and Stretchability. *Adv. Mater.* **2015**, *27*, 3349−3376.
(40) Kaltenbrunner, M.; Sekitani, T.; Reeder, J.; Yokota, T.; Kuribara, K.; Tokuhara, T.; Drack, M.; Schwödiauer, R.; Graz, I.; Bauer-Gogonea, S.; Bauer, S.; Someya, T. An Ultra-Lightweight Design for Imperceptible Plastic Electronics. *Nature* **2013**, *499*, 458−463.
(41) Hubertus, J.; Fasolt, B.; Linnebach, P.; Seelecke, S.; Schultes, G. Electromechanical Evaluation of Sub-Micron NiCr-Carbon Thin Films as Highly Conductive and Compliant Electrodes for Dielectric Elastomers. *Sens. Actuators, A* **2020**, *315*, 112243.
(42) Schultes, G.; Schmid-Engel, H.; Schwebke, S.; Werner, U. Granular Metal−Carbon Nanocomposites as Piezoresistive Sensor Films − Part 1: Experimental Results and Morphology. *J. Sens. Sens. Syst.* **2018**, *7*, 1−11.
(43) Koppert, R.; Uhlig, S.; Schmid-Engel, H.; Göttel, D.; Probst, A.-C.; Schultes, G.; Werner, U. Structural and Physical Properties of Highly Piezoresistive Nickel Containing Hydrogenated Carbon Thin Films. *Diamond Relat. Mater.* **2012**, *25*, 50−58.
(44) Wacker Chemie AG. Data Sheet ELASTOSIL Film 2030. https://www.wacker.com/h/de-de/medias/ELASTOSIL-Film-2030-de-2020.02.26.pdf (accessed 2020 04 27).
(45) Hubertus, J.; Croce, S.; Neu, J.; Rizzello, G.; Seelecke, S.; Schultes, G. Influence of Residual Stresses of Sputtered Thin Film Electrodes for Dielectric Elastomer Applications. *Proceedings of 1st International Electronic Conference on Actuator Technology: Materials, Devices and Applications*, 2020; Vol. *64*, p 2.
(46) Hodgins, M.; York, A.; Seelecke, S. Systematic Experimental Characterization of Dielectric Elastomer Membranes using a Custom-Built Tensile Test Rig. *J. Intell. Mater. Syst. Struct.* **2017**, *28*, 2117−2128.
(47) Carpi, F.; Anderson, I.; Bauer, S.; Frediani, G.; Gallone, G.; Gei, M.; Graaf, C.; Jean-Mistral, C.; Kaal, W.; Kofod, G.; Kollosche, M.; Kornbluh, R.; Lassen, B.; Matysek, M.; Michel, S.; Nowak, S.; O'Brien, B.; Pei, Q.; Pelrine, R.; Rechenbach, B.; Rosset, S.; Shea, H.

Standards for Dielectric Elastomer Transducers. *Smart Mater. Struct.* **2015**, *24*, 105025.
(48) Rizzello, G.; Loew, P.; Agostini, L.; Fontana, M.; Seelecke, S. A Lumped Parameter Model for Strip-Shaped Dielectric Elastomer Membrane Rransducers with Arbitrary Aspect Ratio. *Smart Mater. Struct.* **2020**, *29*, 115030.
(49) Xiang, Y.; Li, T.; Suo, Z.; Vlassak, J. J. High Ductility of a Metal Film Adherent on a Polymer Substrate. *Appl. Phys. Lett.* **2005**, *87*, 161910.
(50) Lambricht, N.; Pardoen, T.; Yunus, S. Giant Stretchability of Thin Gold Films on Rough Elastomeric Substrates. *Acta Mater* **2013**, *61*, 540−547.
(51) Aqrawe, Z.; Boehler, C.; Bansal, M.; O'Carroll, S. J.; Asplund, M.; Svirskis, D. Stretchable Electronics Based on Laser Structured, Vapor Phase Polymerized PEDOT/Tosylate. *Polymers* **2020**, *12*, 1654.
(52) Akbari, S.; Shea, H. Arrays of 100μm x 100μm Dielectric Elastomer Actuators to Strain the Single Cells. *Procedia Eng.* **2011**, *25*, 693−696.
(53) Lacour, S. P.; Jones, J.; Suo, Z.; Wagner, S. Design and Performance of Thin Metal Film Interconnects for Skin-Like Electronic Circuits. *IEEE Electron. Device Lett.* **2004**, *25*, 179−181.
(54) Hsien Low, S.; Lynn Shiau, L.; Lau, G.-K. Large Actuation and High Dielectric Strength in Metallized Dielectric Elastomer Actuators. *Appl. Phys. Lett.* **2012**, *100*, 182901.
(55) Lacour, S. P.; Chan, D.; Wagner, S.; Li, T.; Suo, Z. Mechanisms of Reversible Stretchability of Thin Metal Films on Elastomeric Substrates. *Appl. Phys. Lett.* **2006**, *88*, 204103.
(56) Benslimane, M.; Peter, G. Mechanical Properties of Dielectric Elastomer Actuators with Smart Metallic Copmliant Electrodes. *Smart Structures and Materials 2002: Electroactive Polymer Actuators and Devices*, 2002; Vol. *4695*.
(57) Neu, J.; Croce, S.; Hubertus, J.; Rizzello, G.; Schultes, G.; Seelecke, S. Design and Characterization of Polymeric Domes as Biasing Elements for Dielectric Elastomer Membrane Actuators. *Proc. Actuator.* **2021**, *2021*, 442−445.
(58) Neu, J.; Croce, S.; Hubertus, J.; Schultes, G.; Seelecke, S.; Rizzello, G. Assembly and Characterization of a DE Actuator Based on Polymeric Domes as Biasing Element. *Proceedings of 1st International Electronic Conference on Actuator Technology: Materials, Devices and Applications*; 2020; Vol. *64*, p 24.
(59) Hau, S. High-Performance Dielectric Elastomer Actuators, Ph.D. Dissertation, Universität des Saarlandes: Saarbrücken, 2018 (accessed 2020-04-07).Thesis
(60) Linnebach, P.; Simone, F.; Rizzello, G.; Seelecke, S. Development, Manufacturing, and Validation of a Dielectric Elastomer Membrane Actuator−Driven Contactor. *J. Intell. Mater. Syst. Struct.* **2019**, *30*, 636−648.
(61) Croce, S.; Neu, J.; Hubertus, J.; Seelecke, S.; Schultes, G.; Rizzello, G. Modeling and Simulation of an Array of Dielectric Elestomeric Actuator Membranes. *Proceedings of 1st International Electronic Conference on Actuator Technology: Materials, Devices and Applications*, 2020; Vol. *64*, p 28.

https://doi.org/10.1021/acsami.1c10686
ACS Appl. Mater. Interfaces 2021, 13, 39894−39904